JACS
JOURNAL OF THE AMERICAN CHEMICAL SOCIETY
Article
pubs.acs.org/JACS

CO Oxidation on Supported Single Pt Atoms: Experimental and ab Initio Density Functional Studies of CO Interaction with Pt Atom on θ-Al_2O_3(010) Surface

Melanie Moses-DeBusk,[†] Mina Yoon,[‡] Lawrence F. Allard,[†] David R. Mullins,[§] Zili Wu,[‡,§] Xiaofan Yang,[†] Gabriel Veith,[†] G. Malcolm Stocks,[†] and Chaitanya K. Narula*[,†]

[†]Materials Science & Technology Division, [‡]Center for Nanophase Materials Sciences, and [§]Chemical Sciences Division, Oak Ridge National Laboratory, Oak Ridge, Tennessee 37831-6133, United States

Supporting Information

ABSTRACT: Although there are only a few known examples of supported single-atom catalysts, they are unique because they bridge the gap between homogeneous and heterogeneous catalysis. Here, we report the CO oxidation activity of monodisperse single Pt atoms supported on an inert substrate, θ-alumina (Al_2O_3), in the presence of stoichiometric oxygen. Since CO oxidation on single Pt atoms cannot occur via a conventional Langmuir−Hinshelwood scheme (L−H scheme) which requires at least one Pt−Pt bond, we carried out a first-principles density functional theoretical study of a proposed pathway which is a variation on the conventional L−H scheme and inspired by the organometallic chemistry of platinum. We find that a single supported Pt atom prefers to bond to O_2 over CO. CO then bonds with the oxygenated Pt atom and forms a carbonate which dissociates to liberate CO_2, leaving an oxygen atom on Pt. Subsequent reaction with another CO molecule regenerates the single-atom catalyst. The energetics of the proposed mechanism suggests that the single Pt atoms will get covered with CO_3 unless the temperature is raised to eliminate CO_2. We find evidence for CO_3 coverage at room temperature supporting the proposed mechanism in an in situ diffuse reflectance infrared study of CO adsorption on the catalyst's supported single atoms. Thus, our results clearly show that supported Pt single atoms are catalytically active and that this catalytic activity can occur without involving the substrate. Characterization by electron microscopy and X-ray absorption studies of the monodisperse Pt/θ-Al_2O_3 are also presented.

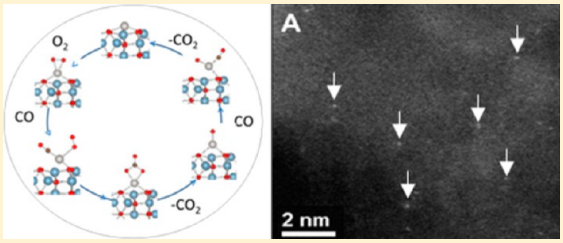

1. INTRODUCTION

The success of emission treatments can be attributed to heterogeneous catalysis where noble metals supported on high surface area oxides, Pt, Rh, and/or Pd supported on γ-alumina and ceria−zirconia, convert toxic gases to inert ones.[1] These noble metal catalysts oxidize CO and hydrocarbons and reduce nitrogen oxides in engine emissions. The widely accepted mechanism of CO oxidation on transition metals, the Langmuir−Hinshelwood scheme (L−H),[2] has been extensively studied by both theoretical[3,4] and experimental methods.[5] The size of the metal particles is considered an important factor in defining the performance of the catalyst.[6−11] A recent detailed study of CO oxidation on supported platinum nanoparticles, by Iglesia et al., shows that CO oxidation can proceed via the L−H mechanism or a CO-assisted, O_2 dissociation step leading to a O−O−C═O intermediate that decomposes to form free CO_2 and chemisorbed O.[12] The smallest size supported particles studied are single atoms supported on metal oxides.[7,11,13−15] Supported single atoms can be isoelectronic with organometallic compounds and might exhibit catalytic activity similar to that of organometallic species in homogeneous environments. For example, density functional theoretical modeling of a palladium single atom supported on magnesium oxide[16] has shown it to be a d^{10} palladium species which would be isoelectronic with a 14-electron bis(triphenylphosphine)-palladium(0), believed to be an intermediate in the catalytic Heck arylation[17] and cyclization reactions.[18] Samples of supported single Pd atoms have indeed been synthesized and shown to be catalytically active for CO oxidation and acetylene cyclotrimerization.[7,19]Another important example of single Pd atom catalysis is heterogeneous hydrogenation by Pd atoms isolated on the Cu surface.[20] Support participation during CO oxidation has been proposed for the Pd/MgO catalyst. Platinum single atoms supported on iron oxide (Pt/Fe_2O_3)[11] have also been synthesized by wet chemical methods and found to be active for catalytic oxidation of CO. The proposed mechanism of CO oxidation on Pt/Fe_2O_3 is a modified L−H scheme where CO absorbs on Pt atoms while oxygen for CO oxidation is provided by the Fe_2O_3 support. Thus, both Pd/MgO and Pt/Fe_2O_3 require support participation for CO oxidation. This raises a question about the catalytic activity of single atoms supported on inert substrates which cannot participate in the catalytic process. To our knowledge, indirect

Received: February 20, 2013
Published: August 2, 2013

references of single-atom catalysis on inert substrates are limited to Pt/γ-Al_2O_3 and Rh/Al_2O_3.[21,22] For Pt/γ-Al_2O_3 catalyst, single Pt atoms are inferred from the structural study of 2-D rafts. IR study of formaldehyde decomposition on Rh/Al_2O_3 allowed the authors to infer single atoms as active species.

We recently reported our results on the first-principles study of group 10 and 11 atoms supported on a θ-alumina surface.[23] We found that Ni, Pt, and Pd are d^{10} species with d−s hybrid character that can interact with the 2p orbital of the supports' surface oxygen. Unlike Pd/MgO and Pt/Fe_2O_3, CO oxidation cannot proceed via the conventional L−H or modified L−H mechanism on Pt/θ-Al_2O_3 because of the inert nature of θ-Al_2O_3. However, all three of these species find analogues in organometallic chemistry, for example, $(Ph_3)_2M$, where M = Ni, Pd, or Pt.[24−26] In analogy with organometallic counterparts, the supported single atoms of Ni, Pd, and Pt can be considered 14-electron complexes. As such, the supported single atoms should be catalytically active, and the catalytic reactions on both supported atoms and their organometallic counterparts should, in principle, follow identical pathways. In order to demonstrate that supported single atoms on inert substrates are indeed catalytically active, we synthesized single Pt atoms supported on θ-alumina by wet chemical routes and found them to be catalytically active for CO oxidation. The results are presented here.

Successful formation of samples of single supported Pt atoms was confirmed by aberration-corrected electron microscopy (ACEM). In situ infrared CO absorption studies and EXAFS also support formation of single supported Pt atoms. The catalyst is catalytically active, as seen by its ability to oxidize CO. Considering the isoelectronic nature of Pt/θ-Al_2O_3 with $(Ph_3)_2M$, we propose a CO-oxidation pathway that involves intermediates that have been observed in reactions of $(Ph_3)_2Pt$ with O_2, CO, and CO_2. The proposed mechanism can be considered a variation of the L−H mechanism that does not require support participation.

2. EXPERIMENTAL METHODS

2.1. Pt/θ-Al_2O_3 Preparation. Samples of chloroplatinic acid were purchased from Aldrich and used without further purification. θ-Al_2O_3 was synthesized from an alumina sol−gel by procedures described in the literature.[27,28] For catalyst preparation, a sample of alumina powder was added to an aqueous solution of chloroplatinic acid as it was stirred. Water was gradually evaporated with mild warming in an oil bath over ∼30 h while keeping the mixture stirred or on a rotovap with mild vacuum, resulting in a free-flowing powder. Powder was transferred to an alumina crucible, pyrolyzed in an ambient environment oven at a 1 °C/min to 450 °C, and held at that temperature for 4 h to obtain the catalyst samples.

2.2. Pt/θ-Al_2O_3 Characterization. X-ray powder diffraction patterns were recorded on a Scintag PAD-V diffractometer. BET surface areas of alumina powders were obtained on a Quantachrome Autosorb system. Transmission electron micrographs of catalyst samples were recorded on a Hitachi HD-2000 and a JEOL 2200FS FEG 200kv scanning transmission electron microscope (STEM). The JEOL STEM with a hexapole aberration-corrector (ACEM) in the high-angle annular dark-field (HA-ADF) mode was used for atomic resolution images.

X-ray absorption spectroscopy (XAS) data were recorded at the Pt L_{III}-edge (11564 eV) at beamline X19a at the National Synchrotron Light Source, Brookhaven National Laboratory. A Si(111) double-crystal monochromator was used and detuned by 30% to reject higher harmonics. XAS was measured simultaneously in fluorescence and transmission modes. Fluorescence was measured using a large area passivated implanted planar silicon (PIPS) detector oriented perpendicular to the upcoming beam. Ion chambers for measuring I_o and I_t were filled with nitrogen and argon, respectively. Pt absorption was measured out to k = 16.

Samples were ground to a fine powder, mixed with BN, and pressed into a 13 mm diameter pellet. The typical absorbance of the Pt, $\mu(x)$, was less than 0.1. Pellets were mounted in a Nashner-Adler reaction cell.[29] A gas flow pipe terminated near the sample's surface to allow reduction of the sample in a mixture of 5% H_2/He. Measurements were recorded while the sample was in pure He at 25 °C < T < 30 °C. The sample was heated by a cartridge heater inserted in the sample mount. A Pt foil was placed downstream of I_t and in front of an additional ion chamber (I_r) during measurements as an energy reference.

Programs ATHENA (version 0.8.061) and ARTEMIS (version 0.8.014) were used to reduce and fit the data, respectively.[30] Data reduction consisted of pre-edge subtraction, background determination, normalization, and spectral averaging. k^3-weighted EXAFS functions, $X(k)$, were Fourier transformed and fit in R space. EXAFS was fit over the first-shell neighbors, R = 1.0−3.0 Å. The sample containing 1% Pt was fit using k = 2−15 $Å^{-1}$. Poor signal-to-noise limited the usable range for the 0.18% Pt sample to k = 2−14 $Å^{-1}$. This resulted in 16 and 15 independent points in the 1% and 0.18% samples, respectively. The as-received 1% Pt sample was fit over just the Pt−O region (1−2 Å) to derive the best value for σ^2 for this scattering pair. Likewise, the reduced 1% Pt sample was fit over just the Pt−Pt region (2−3 Å) to derive the best value for σ^2 for this pair. These values were then constrained in all subsequent fits in order to minimize the correlation between N and σ^2 in the reported results. E_0, the inner potential correction, was fit using a single variable for all scattering pairs. The total number of free variables was therefore five or seven depending on whether the EXAFS was fit to two or three scattering pairs, respectively.

2.3. CO Oxidation on Pt/θ-Al_2O_3. The activity of the catalysts was determined using a custom-built flow reactor to monitor conversion of carbon monoxide to carbon dioxide. Powders of catalyst (0.086g) were loaded into a quartz U tube (i.d.= 4 mm) and supported on both ends with glass wool. A mixture of 27 sccm/min comprising high-purity helium (99.99%, Air Liquide), oxygen (ultrahigh purity, Air Liquide), and carbon monoxide (research grade, Matheson, stored in an aluminum cylinder) was delivered from three Sierra Instruments Mass Flow valves at rates of 25, 1, and 1 sccm, respectively. This corresponds to a space velocity of 20 930 h^{-1} (18 837 mL h^{-1} g_{cat}^{-1}) for all catalyst samples. The U-tube reactor was placed in a custom-made Mellen furnace, heated at a rate of 1.644 °C/min, and held at 260 °C for 10 min before letting the furnace cool down. The temperature of the catalyst bed was determined using an embedded K-type thermocouple. Product evolution was monitored with an Ametek Dymaxion mass spectrometer (0−200 amu range). The plots show CO conversion as a function of temperature where the temperature is that of the catalyst bed and CO conversion is calculated as $[CO_2]/([CO] + [CO_2])$.

In order to compare platinum catalysts, turnover frequencies (TOF) were calculated at both 20% CO conversion and 200 °C based on dispersions calculated from irreversible H_2 chemisorption. Here, TOF is moles of CO converted per second divided by the total moles of surface platinum atoms and described in more detail in the Supporting Information.

2.4. Infrared Study during CO Adsorption. In situ diffuse reflectance Fourier transform infrared spectroscopy (DRIFTS) measurement was performed on a Nicolet Nexus 670 spectrometer equipped with a MCT detector cooled by liquid nitrogen and an in situ chamber (HC-900, Pike Technologies) with capability to heat samples to 900 °C. The exiting stream was analyzed by an online quadrupole mass spectrometer (QMS) (OmniStar GSD-301 O2, Pfeffer Vacuum).[31] All samples studied by DRIFTS were first heated to 150 °C under a flow of 100 sccm of 4% H_2 in helium at a rate of 3 °C/min and held at that temperature for 45 min. Samples were then cooled to the desired temperature under a flow of 100 sccm of helium. Spectra were obtained in a flowing helium environment on samples

after exposure to 1.3% CO in helium for 5 min followed by 5 min He purging (100 sccm). Space velocity conditions were kept constant from sample to sample. Each DRIFT spectra was recorded at a frequency of 300 scans per 10 min. As a control experiment, we examined CO adsorption on θ-Al_2O_3 and found no CO adsorption.

2.5. Computational Methods. Our total energy calculations are based on ab initio density functional theory (DFT) as implemented in the Vienna Ab Initio Simulation Package (VASP).[32−34] A generalized gradient approximation (GGA) in the Perdew−Wang-91 form[33−36] was employed for the electron exchange and correlation potential. Kohn−Sham equations were solved using the projector-augmented wave (PAW) approach for describing electronic core states.[37,34] The plane-wave basis set was truncated at a kinetic energy cutoff of 500 eV. A Gaussian smearing function with a width of 0.05 eV was applied near the Fermi level. Ionic relaxations were considered converged when the forces on the ions were <0.03 eV/Å. Details of construction of the (010) θ-alumina surface have been described previously by us.[23] Briefly, a charge neutral 2 × 4 supercell was constructed from optimized bulk θ-alumina containing 180 atoms. Cations and anions are aligned on the same planes parallel to the surface, and both O_h and T_d aluminum are exposed. The optimized location of Pt is between two oxygen atoms on adjacent rows. The total energies of various optimized species are summarized in Table 1.

Table 1. Total Energy of Optimized Structures

structure	total energy (eV)	structure	total energy (eV)
Pt/θ-Al_2O_3	−1315.7614	VI	−1345.8156
I	−1326.4198	VII	−1337.2274
II	−1320.6408	CO	−14.7764
III	−1332.4053	CO_2	−22.9544
IV	−1348.4249	O_2	−8.7847
V	−1343.1760	O	−0.09153

Results were compared with all-electron first-principles quantum mechanical calculations using FHI-aims code.[39] We employed standard "tight" settings including numerical atom-centered orbitals basis set of *tier1* for Al and Pt and *tier2* for C and O.[35] The exchange-correlation potential of the Perdew−Burke−Ernzerhof (PBE) version of the generalized-gradient approximation (GGA)[40] was used, and also relativistic correction within a Zora scalar scheme[39] was applied.

The k-point sampling was done with a 4 × 2 × 4 number of mesh points for bulk and adopted large vacuum size (>30 Å) in the supercell configuration. We evaluated the full vibrational spectra of the films and calculated the vibrational free energy (F_{vib}) using the harmonic approximation[41] as

$$F_{vib} = \int d\omega g(\omega)\{\hbar\omega/2 + k_B T \ln[1 - \exp(-\hbar\omega/k_B T)]\} \quad (1)$$

where k_B is the Boltzmann constant and $g(\omega)$ is the phonon density of states depending on vibrational frequencies (ω). Here, we take into account all vibrational modes contributing to the atomic degree of freedom. The Gibbs free energy (G) is a measure for the structural stabilities at a finite T and pressure (P) and can be written as $G = U + PV + F_{vib}$, where U is the internal energy including the zero-point energy and V is the volume of the films. We compare the changes in the Gibbs free energy (ΔG) of Pt−alumina films upon gas adsorption. Here we assume that the changes in film volumes are negligible. Our reference systems are Pt−alumina films with the same crystalline orientation as gas adsorbed films and individual ideal gas in its most preferred form. The ideal gas equation is applied for the chemical potential of the reference gas. The change of the chemical potential of the given gas is calculated using the internal energies including from the electronic contribution and the zero-point energies.

3. RESULTS AND DISCUSSION

3.1. Evidence for Monoatomic Pt Dispersion in Pt/θ-Al_2O_3. Samples for this study were prepared by impregnation of chloroplatinic acid on θ-alumina. Samples with 0.18%, 1.0%, and 2% Pt ($_{wt}$%) loadings are referred to as 0.18% Pt/θ-Al_2O_3, 1.0% Pt/θ-Al_2O_3, and 2.0% Pt/θ-Al_2O_3, respectively. In order to prepare Pt/θ-Al_2O_3 with practically no single atoms, a sample of 2.0% Pt/θ-Al_2O_3 was sintered at 650 °C in ambient atmosphere and the sample is referred to as 2.0% Pt/θ-Al_2O_3-650. In addition, a 0.12% Pt/θ-Al_2O_3 sample was also prepared for comparison of EXAFS data for samples with 0.18 and 1.0% Pt loading. The solution method with low loading appears to be the simplest method to prepare monoatomically dispersed platinum on θ-alumina.[11] The X-ray powder diffraction patterns (XRD) of θ-Al_2O_3 matches with JCPDS 23-1009, confirming its phase purity. Employing the Scherer formula, the average size of θ-Al_2O_3 particles was calculated to be 27.6 nm. The BET surface area of θ-Al_2O_3 is 189 m^2/g. After Pt loading by the standard wet impregnation method, the surface area did not change.

Atomic level imaging, by ACEM, of 0.18% Pt/θ-Al_2O_3 shows only single atoms and no rafts were found after examination of multiple areas. Unlike the Pt/FeO_x system,[11] platinum single atoms do not appear to be embedded in alumina and move on the surface under the beam over time. The 1.0% Pt/θ-Al_2O_3 (Figure S1, Supporting Information) and 2.0% Pt/θ-Al_2O_3 (Figure 1) samples exhibit two distinct Pt environments, single

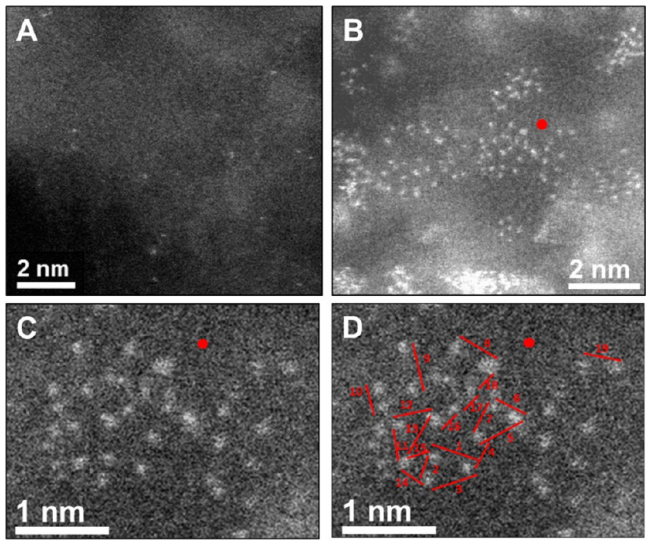

Figure 1. ACEM HAADF-STEM images 0.18% Pt/θ-Al_2O_3 and 2.0% Pt/θ-Al_2O_3 (A and B, respectively). (C and D) Identical enlargements of a portion of B with the red dot used as a reference point. Numbers in image D correspond to various observed Pt−Pt distances summarized in Table 2.

Pt atoms and 10−20 atom agglomerates. Close examination of Pt−Pt distances in the atom agglomerates in ACEM of 2.0% Pt/θ-Al_2O_3 reveals that most of the platinum atoms are more than 3 Å apart from each other, suggesting that the agglomerates predominately consist of single platinum atoms which are probably bonded through oxygen (Table 2).

These ACEM-STEM pictures of 0.18% Pt/θ-Al_2O_3 and 1.0% Pt/θ-Al_2O_3 are very similar to the ones recently reported for Pt/Fe_2O_3 and Pt/γ-Al_2O_3 systems, respectively.[11,21] It is important to point out that the z dimension in the micrographs of 1.0% Pt/θ-Al_2O_3 and 2.0% Pt/θ-Al_2O_3 are not known, the distances are only the x−y projection. The Pt atoms could exist on the front surface, back surface, or within the alumina

dx.doi.org/10.1021/ja401847c | J. Am. Chem. Soc. 2013, 135, 12634−12645

Table 2. Pt−Pt Distances in Pt Rafts of 2.0% Pt/θ-Al_2O_3

marker	distance (Å)	marker	distance (Å)
1	3.82	11	4.00
2	2.61	12	3.80
3	4.53	13	5.53
4	3.45	14	3.28
5	4.35	15	3.30
6	2.60	16	2.27
7	3.64	17	2.79
8	3.97	18	3.14
9	4.87	19	3.65
10	2.09		

particles. Therefore, the Pt−Pt distances are likely much bigger than the table values. However, they do appear to be monoatomically dispersed. The monatomic dispersion seen in the 0.18% sample is not surprising since monatomic Pt dispersion has been observed at this Pt loading level for Pt/Fe_2O_3. Also, Kwak et al.[38] point out that monatomic dispersion of Pt is normal for samples with a Pt loading of 1% or less and show 2-dimensional rafts of Pt atoms bonded through oxygen (Pt−O−Pt bonds) at higher loadings of platinum on γ-Al_2O_3. The Pt−Pt distances in these rafts are estimated to be 2.7−2.8 Å. These rafts ultimately form 3-dimensional platinum particles upon sintering.[21]

X-ray adsorption near-edge spectra (XANES) for the 0.18% Pt/θ-Al_2O_3 and 1.0% Pt/θ-Al_2O_3 are shown in Figure 2. The XANES spectrum from fresh 1.0% Pt/θ-Al_2O_3 (Figure 2 right, black line) indicates that the Pt was highly oxidized based on the intensity of the "white line" at 11 568 eV.[42] After heating the sample in He at 150 °C for 30 min, the Pt became slightly less oxidized as indicated by the decrease in the white line intensity (Figure 2 right, red line). After reduction in 5%H_2/He at 150 °C for 60 min, the Pt became considerably reduced (Figure 2 right, blue line).

The white line from the fresh 0.18% Pt/θ-Al_2O_3 (Figure 2 left, black line) is indistinguishable from PtO_2. Note that while the 1.0% Pt/θ-Al_2O_3 sample is highly oxidized, the white line intensity is slightly lower than the PtO_2 reference. After exposure to 5%H_2/He at 150 °C for 60 min, the spectrum of 0.18% Pt/θ-Al_2O_3 was unchanged (Figure 2 left, blue line), indicating that the Pt remained fully oxidized.

The nonphase-corrected, k^3-weighted EXAFS at the Pt L_{III}-edge for the 0.18% Pt/θ-Al_2O_3 and 1.0% Pt/θ-Al_2O_3 are shown in Figure 3. Consistent with the XANES results (Figure 2), the EXAFS of 0.18% Pt/θ-Al_2O_3 indicates very little difference between the fresh sample and after it was reduced in 5%H_2/He at 150 °C. The dominant feature in both is Pt−O. The best fit for the fine structure indicates that the Pt has 6 oxygen neighbors at 1.94 Å (Table 3). The feature at 2.72 Å is barely above the noise level and could be considered insignificant as reported previously for single Pt atoms on α-Al_2O_3 single crystals.[43] EXAFS and XANES results were found to be reproducible on a fresh batch of sample and the feature at 2.72 Å did not change in intensity. In our efforts to ensure that this feature is indeed noise, we prepared a sample with 0.12% platinum loading (0.12% Pt/θ-Al_2O_3) (Figure S2, Supporting Information) and found the feature at 2.72 Å to be barely above noise level. Considering that our synthetic method involves impregnation and decomposition of chloroplatinic acid, it would be highly unlikely to keep Pt rafts, if present, at a constant level to give rise to the feature at 2.72 Å. However, this feature can be fitted to Pt−Pt interaction (N 4.1 (1.6), R(0.02) 2.72, σ^2 0.007, and ΔE_0 18). This feature definitely is different from the feature at 2.7 originating from Pt−Pt interaction in rafts in 1.0% Pt/θ-Al_2O_3 (Table 3).

In analogy with Pt/FeO_x, which shows Pt−O and Pt−Fe interaction in its EXAFS,[11] isolated Pt atoms bonded to the Al_2O_3 would result in Pt−O and Pt−Al nearest neighbors. In the EXAFS of Pt/FeO_x, the Pt−O and Pt−Fe features are seen at ∼1.7 and ∼2.5 originating from Pt atom bonding to oxygen of the substrate and the interaction of Pt with the Fe of the substrate. In 0.18% Pt/θ-Al_2O_3, Pt−Al scattering was not evident when we modeled with Pt−Al bonds at 2.4 Å. On average, the results suggest that 0.18% Pt/θ-Al_2O_3 is predominantly isolated atoms. Thus, the results of EXAFS, XANES, and ACEM support the presence of single platinum atoms supported on θ-Al_2O_3 surface. This bonding picture is different from that reported for Pt/FeO_x where platinum atoms replace iron in a iron oxide substrate.

The most intense feature in the EXAFS of the fresh 1.0% Pt/θ-Al_2O_3 (Figure 3 right, black line) occurs near 1.6 Å. This feature can be fit to nearest neighbor oxygen at a distance of 1.99 Å. The phase shift places the peak position at a distance that is shorter than the actual position. The best fit indicates 4.8 nearest O neighbors surrounding the Pt (see Table 3). The next largest feature near 2 Å can be fit to two Al nearest neighbors at a distance of 2.39 Å. This feature can also be fit to

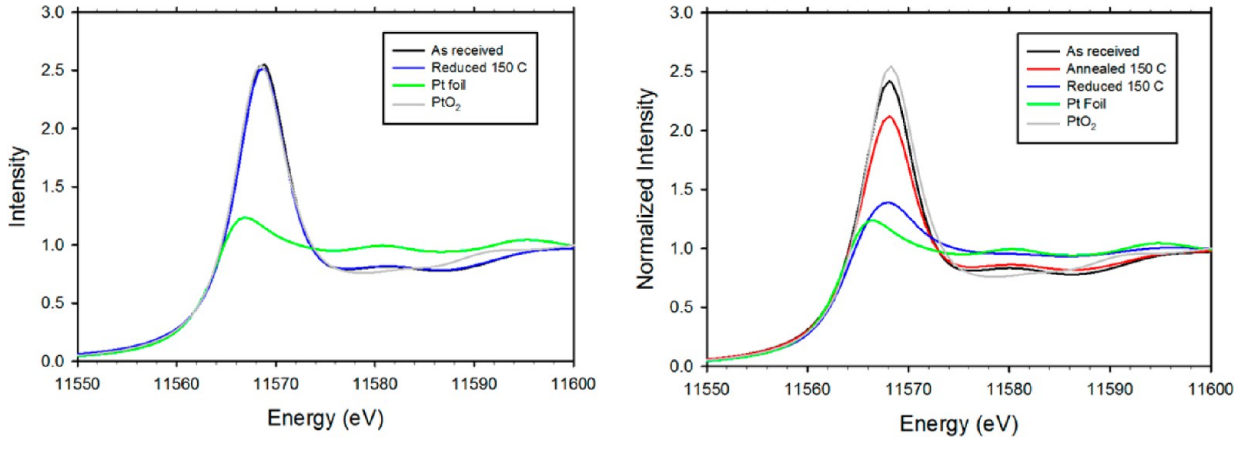

Figure 2. Pt L_{III}-edge XANES for 0.18% Pt on θ-Al_2O_3 (left) and 1.0% Pt on θ-Al_2O_3 (right).

dx.doi.org/10.1021/ja401847c | J. Am. Chem. Soc. 2013, 135, 12634−12645

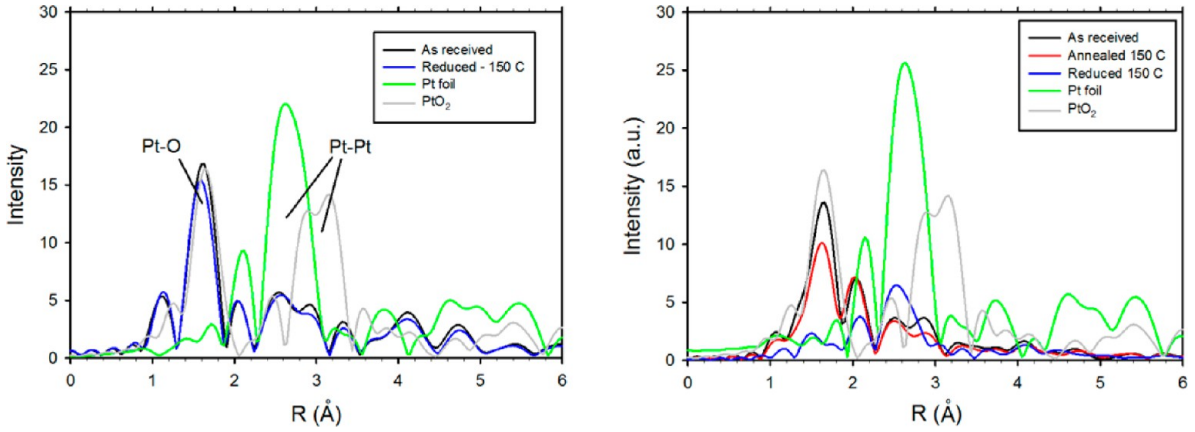

Figure 3. Non-phase-corrected, k^3-weighted Fourier transform of Pt L_{III}-edge EXAFS for 0.18% Pt on θ-Al_2O_3 (left) and 1.0% Pt on θ-Al_2O_3 (right).

Table 3. EXAFS Fitting Results for Pt on θ-Al_2O_3 and Several Reference Materials[a]

sample	neighbor	N	R (Å)	σ^2 (Å^2)	ΔE_0 (eV)
0.18% Pt/θ-Al_2O_3 as received	O	6.2	1.94	0.003	18
0.18% Pt/θ-Al_2O_3 reduced 150 °C	O	5.7	1.93	0.003	17
1.0% Pt/θ-Al_2O_3 as received	O	4.8	1.99	0.003	10
	Al	2.0	2.39	0.003	10
	Pt	1.9	2.79	0.007	10
1.0% Pt/θ-Al_2O_3 annealed 150 °C	O	2.3	1.97	0.003	7
	Al	2.1	2.37	0.003	7
	Pt	2.4	2.75	0.007	7
1.0% Pt/θ-Al_2O_3 reduced 150 °C	O	0.6	1.93	0.003	4
	Pt	5.6	2.73	0.007	4
Pt foil (25 °C)	Pt	12	2.72	0.005	18
α-PtO_2	O	6	2.02	0.002	12
	Pt	6	3.10	0.002	12

[a] N, R, σ^2, and ΔE_0 are the coordination number, interatomic distance, Debye–Waller factor, and shift in the edge energy. Errors in the fitting parameters are N ± 20% (except Pt foil and PtO_2 which were fixed), R ± 0.02 Å, σ^2 ± 20%, and ΔE_0 ± 20%.

a Pt–O scattering pair at a similar distance; however, computational modeling as well as chemical intuition suggests that this scattering pair is unlikely. Finally, there is intensity apparent between 2.3 and 3.1 Å. The only pair that results in even a nominally reasonable fit to the data is Pt–Pt at a distance of 2.79 Å arising from Pt–O–Pt linkages in view of the XANES data that indicated that the Pt was oxidized and not metallic.

When 1.0% Pt/θ-Al_2O_3 is annealed at 150 °C in He, the Pt–Al and Pt–Pt coordination and distances remain essentially unchanged. However, the Pt–O coordination decreases from ca. 4.8 to 2.3. This is consistent with the XANES (Figure 2), where the decrease in the white line intensity indicates a decrease in the oxidation of the Pt. Presumably, annealing the sample resulted in loss of terminal O capping the Pt on the Al_2O_3. Reducing the sample at 150 °C in 5%H_2/He produced a significant change in the EXAFS. The Pt–O feature decreased and the Pt–Pt increased. The best fit for the Pt–O indicated at most one Pt–O neighbor at a distance of 1.93 Å. The apparent Pt–Pt coordination increased to ca. 5.6 at a distance of 2.73 Å. A reasonable fit was obtained without inclusion of a Pt–Al scattering pair. As with the other fitting results, the coordination numbers are averages for all Pt environments over the entire sample and could be greater or smaller in any given type of structure. These results indicate sintering in the reducing atmosphere.

Increasing the platinum concentration to 2% in 2.0% Pt/θ-Al_2O_3 does not have a significant impact on the Pt agglomerates, and the ACEM images of the 2.0% Pt/θ-Al_2O_3 sample resemble those of 1.0% Pt/θ-Al_2O_3 with single atoms and 10–20 atom rafts (Figure 4, left, and Figure S1, Supporting Information). As expected, thermal treatment leads to extensive sintering, and the images of 2.0% Pt/θ-Al_2O_3-650 show primarily well-defined Pt particles, although occasional rafts and very large particles can be seen in ACEM images (Figure 4 right, Figure S3, Supporting Information).

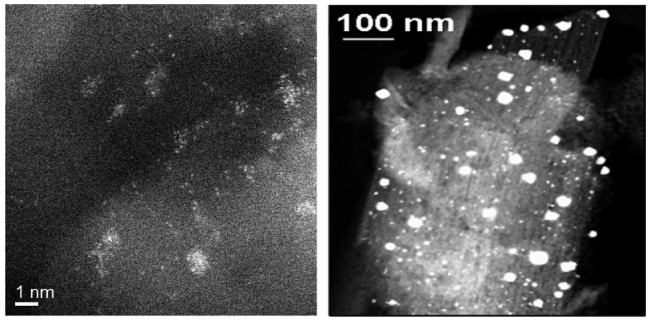

Figure 4. HAADF-STEM images of 2.0% Pt/θ-Al_2O_3 (left) and 2.0% Pt/θ-Al_2O_3-650 (right). (Left) Obtained using an aberration-corrected microscope.

3.2. CO Oxidation on Pt/θ-Al_2O_3. CO oxidation experiments were carried out at a fixed flow mixture of CO, oxygen, and helium at a constant hourly space velocity (constant weight of catalyst). CO oxidation on 0.18% Pt/θ-Al_2O_3, 1.0% Pt/θ-Al_2O_3, and 2% Pt/θ-Al_2O_3 initiates at approximately 200, 175, and 130 °C, respectively (Figure 5). The results clearly show that supported single Pt atoms are catalytically active for oxidation of CO. In comparison, CO oxidation on 2% Pt/θ-Al_2O_3-650 which contains predominantly large particles initiates at ~200 °C, which is significantly higher than the comparable 2% Pt/θ-Al_2O_3 sample.

The temperature of reaction was raised to 260 °C, and after 10 min the sample of 0.18% Pt/θ-Al_2O_3 was taken out of the CO oxidation reactor and examined by ACEM, which showed

dx.doi.org/10.1021/ja401847c | J. Am. Chem. Soc. 2013, 135, 12634–12645

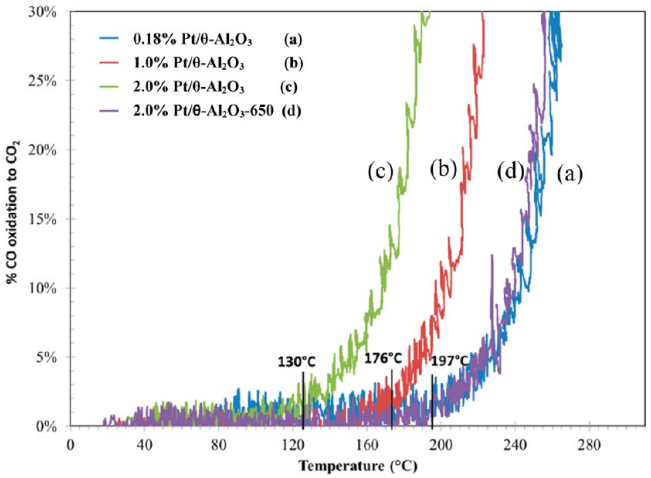

Figure 5. CO conversion to CO_2 for the Pt/θ-Al_2O_3 samples.

that sample is still predominantly single atoms, although rare particles were also seen (Figure S4, Supporting Information). A trend to lower activation temperatures for catalytic oxidation of CO is observed as the loading of the catalytically active Pt species increases. For turnover frequency calculation, we determined Pt dispersion in our samples which was near 100% for each of the 0.18%, 1.0%, and 2.0% Pt/θ-Al_2O_3 samples but dropped for 2% Pt/θ-Al_2O_3-650 as expected due to the large Pt particles. Turnover frequencies based on dispersion estimates were calculated at two conditions, 20% CO oxidation and 200 °C, for the purpose of performance comparison, Table 4. A detailed description of dispersion and TOF calculation can be found in the Supporting Information.

Table 4. Comparison of TOFs

	Pt loading (wt%)	CO_{ox} at 200 °C	TOF x 10^2 (s^{-1})[a]	temp at 20% CO_{ox}	TOF $\times$ 10^2 (s^{-1})[a]
0.18% Pt/θ-Al_2O_3	0.18	1.40%	1.3	251 °C	18.7
1.0% Pt/θ-Al_2O_3	1.0	8.1%	1.4	212 °C	3.4
2.0% Pt/θ-Al_2O_3	2.0	59.9%	5.1	182 °C	1.7
2.0% Pt/θ-Al_2O_3-650C	2.0	0.9%	0.2	248 °C	3.4

[a]TOF was calculated based on Pt dispersion (mol CO_{ox}/mol sutface Pt). Pt dispersion was extrapolated from H_2 chemisorption strong/difference isotherms for both 2.0% Pt samples. Dispersion of 0.18% Pt was estimated by the Pt particle size according to $D = 1/d_{pt}$.

Comparison of TOFs at 20% CO conversion for our samples of 0.18%, 1.0%, and 2.0% Pt/θ-Al_2O_3 shows that 0.18% Pt/θ-Al_2O_3 is the most active platinum, but 20% CO conversion occurs at different temperatures.

3.3. CO Oxidation on a Single Pt Atom on θ-Al_2O_3. *Theoretically Proposed Mechanism.* As mentioned earlier, the conventional Langmuir–Hinshelwood mechanism is not applicable for CO oxidation on single atoms in 0.18% Pt/θ-Al_2O_3 since adjacent sites for CO and O_2 adsorption are not available. Also, the variation of the Langmuir–Hinshelwood mechanism, proposed for single atoms of Pd and Pt in Pd/MgO and Pt/Fe_2O_3, are not applicable since θ-Al_2O_3 is inert and cannot host CO or oxygen in the manner of MgO or Fe_2O_3. Inspired by homogeneous catalysis by organometallic complexes, we propose a variation of the L–H scheme for supported single Pt atoms on an inactive support. The mechanism builds upon our recently published[23] first-principles study of Pt atoms supported on a θ-Al_2O_3 (010) surface. As described previously, a charge neutral 2 × 4 supercell was constructed from optimized bulk θ-alumina-containing 180 atoms. Cations and anions are aligned on the same planes parallel to the surface, and both O_h and T_d aluminum are exposed. We found that a platinum atom adsorbs on the θ-Al_2O_3 (010) surface in a bridging position between 2 oxygen atoms, which are each bonded to one Al_{td} and one Al_{oh} atom, and is in a d^{10} oxidation state. Thus, Pt/θ-Al_2O_3 (010) is isoelectronic with bis(triphenylphosphine)platinum(0), $(Ph_3P)_2Pt$, which is a d^{10} 14-electron complex.[26] Since $(Ph_3P)_2Pt$ is a known catalyst, we expected the isoelectronic alumina-supported Pt to also be catalytically active, and our experimental observation of CO oxidation confirms this suggestion.

For experimentalists, it is not surprising that this "14-electron platinum atom" undergoes oxidative addition of oxygen and one can expect the experimentally synthesized single supported Pt atom to be oxidized. Indeed, we find the experimentally synthesized single supported atoms, 0.18% Pt/θ-Al_2O_3, to be oxidized by XANES as described in the previous section. The 0.18% Pt/θ-Al_2O_3 sample shows six oxygen neighbors when freshly prepared and starts to lose some oxygen upon reduction. Oxidative addition of oxygen is also a key step in platinum particle catalyzed oxidation reactions and has been a subject of several theoretical investigations.[44−47] Experimental evidence for various physisorbed and chemisorbed oxygen species on Pt particles also exists.[48] In general, molecular oxygen adsorbs on two neighboring Pt atoms on the surface of the Pt particle, and dissociative adsorption leads to atomic oxygen on the Pt surface. However, single Pt atoms cannot adsorb molecular oxygen in such a mode. Previous studies on oxygen adsorption on supported single atoms are limited to a recent theoretical investigation of atomic oxygen adsorption on a Pt/α-alumina system.[49] There are two possible bonding modes for oxygen: side-on chelating and terminal monodentate. We find that the energetically preferred mode for oxygen bonding to Pt is side-on chelating (Scheme 1).

Scheme 1. Interaction of Oxygen with Pt/θ-Al_2O_3

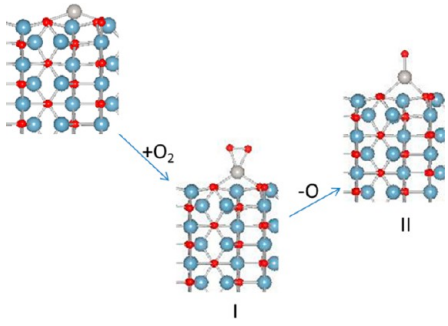

The bonding of oxygen on platinum single atoms by side-on chelating has been observed previously in a 16-electron complex,[50,51] $(Ph_3P)_2Pt(O_2)$, formed from oxidation of $(Ph_3P)_2Pt$. Our attempts to optimize a structure with oxygen bonded to the platinum of Pt/θ-Al_2O_3 in a terminal monodentate mode were unsuccessful as the oxygen molecule continued to bend toward platinum, suggesting that the chelating bonding mode is preferred with both oxygen atoms bonded to platinum.

dx.doi.org/10.1021/ja401847c | J. Am. Chem. Soc. 2013, 135, 12634−12645

The optimized structure, configuration **I** (see Scheme 1 and Figure S5, Supporting Information), exhibits no magnetization suggesting no unpaired electron and the Pt is either in a d^8 or a d^{10} oxidation state. The density of states analysis of Pt/θ-alumina (Figure 6) clearly shows unoccupied d_{xy} orbitals

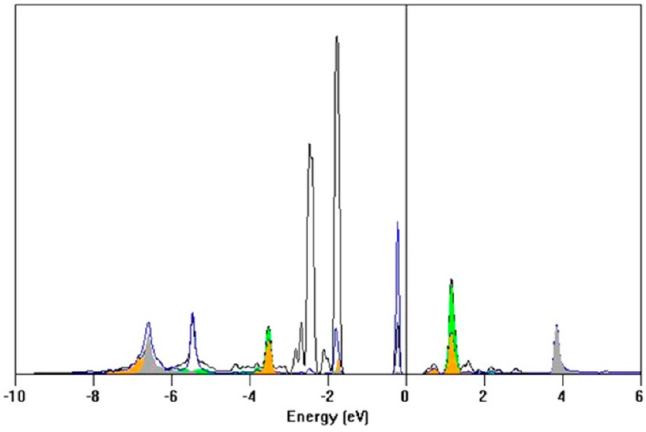

Figure 6. Projected density of states (PDOS) plots of Pt d orbitals (black) and adsorbed oxygen 2p orbitals (blue) for configuration I (see Scheme 1). Filled green area is the contribution of $5d_{xy}$, and filled yellow and gray areas are the contributions of p_y and p_x, respectively. Here, energy (E) is with respect to the Fermi level (E_F).

supporting a d^8 structure. This bonding picture, (alumina)Pt-(O_2), is similar to that of $(Ph_3P)_2Pt(O_2)$. In analogy to $(Ph_3P)_2Pt(O_2)$,[51] the molecular orbital picture of chelating oxygen bonded to Pt/θ-alumina exhibits occupied ligand σ and π orbitals, four 5d orbitals from Pt, O_2 π^* orbitals, and unoccupied $5d_{xy}$ of Pt and σ^* of O_2. Molecular adsorption of O_2 results in weakening of the Pt interaction with surface oxygen anions.

These weakened interactions are inferred from the longer (~0.09 Å) platinum bonds with surface oxygen atoms. The bond distance between platinum and the atoms of the adsorbed molecular oxygen are 1.98 Å, which compares favorably with that of 2.00 Å in $(Ph_3P)_2Pt(O_2)$. The O−O bond distance of 1.44 Å in (alumina)Pt(O_2) is shorter than the O−O distance of 1.50 Å observed in $(Ph_3P)_2Pt(O_2)$ due primarily to the large O−Pt−O angle of 112.9° created by the Pt bonds to surface oxygen atoms (cf. P−Pt−P bond of 101.7° in $(Ph_3P)_2Pt(O_2)$), thereby forcing oxygen atoms of the adsorbed oxygen molecule closer. Compared to single Pt atoms, the bonds of oxidized single platinum with surface oxygen are longer, suggesting weakening of the surface interaction with Pt upon oxidation. The absorption energy of Pt(O_2) on alumina surface is −57.48 kcal/mol, which is 17.77 kcal/mol less than the absorption energy of Pt atoms[23] on the alumina surface. These data suggest that oxidized Pt atoms on the alumina surface are less strongly adsorbed than Pt atoms. These results are also consistent with a previous study on gas-phase single atoms which shows that single Pt atoms exist as oxidized species and will require very low oxygen pressure and high temperature to exist as a single atom.[52]

Weakening of platinum surface bonds in configuration **II** is evident from 0.2 Å longer platinum bonds with the surface oxygen atoms of alumina. The 1.79 Å Pt−O bond distance of the atomic oxygen bonded to platinum compares favorably with 1.79 Å reported for the atomic oxygen bond with platinum in the Pt/α-alumina system.[49] The magnetization centered on the Pt−O fragment suggests unpaired electrons. The PtO fragment binding energy to the θ-Al_2O_3 surface is −1.66 eV. The magnetization is predominantly centered on Pt and atomic oxygen. Electronic density of states analysis shows partially occupied Pt d_{xy} and d_{yz} orbitals, suggesting a high-spin Pt structure (Figure 7).

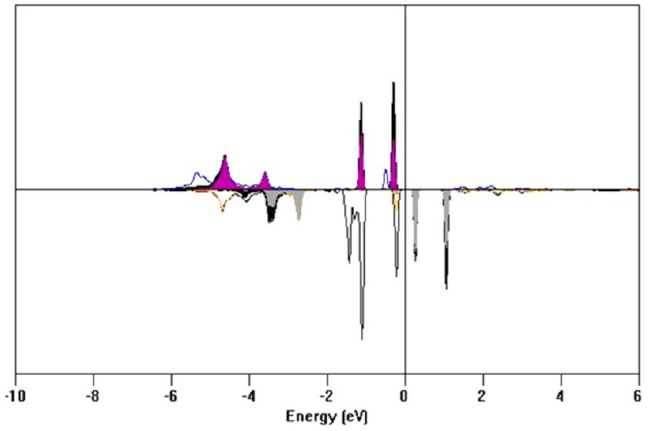

Figure 7. PDOS for Pt d orbitals (black) and adsorbed oxygen 2p orbitals (blue and yellow) of configuration **II** (see Scheme 1). Filled black area is the contribution of $5d_{xy}$ and $5d_{yz}$, and filled violet and gray areas are contributions of p_z and p_x for each.

Dissociative adsorption of oxygen molecules is unlikely because of the lack of another Pt atom in proximity, and O_2 cannot dissociate to release a single oxygen atom. Our analysis also shows that dissociative adsorption of O_2 is an endothermic step (5.68 eV for the loss of O from I) and an energetically unfavorable pathway for oxygen adsorption on Pt/θ-Al_2O_3.

In addition, our all-electron DFT calculations combined with the first-principles thermodynamic approach show that configuration **II** is accessible only at a very low oxygen pressure (P) ($P < 10^{-16}$ bar) and high temperatures (see Figure 8a). Differences in chemical potential between oxygen in configurations **I** and **II** are still over 2.5 eV at 2000 K at P = 1 bar (Figure 8b).

The L−H mechanism for CO oxidation requires CO and oxygen to be adsorbed on the Pt surface on adjacent platinum locations. Since single atoms do not have two available sites, it is necessary for both CO and oxygen to adsorb simultaneously on the atom. Such an intermediate has been proposed for CO oxidation on Pd single atoms.[7] Prior to investigating such an intermediate, we optimized the CO interaction with the platinum atom on Pt/θ-alumina, as shown in Scheme 2.

Absorption of one molecule of CO on Pt in configuration **III** results in weakening of Pt adsorption on the surface as evident from the lengthening of surface Pt−O bonds by ~0.2 Å. The lack of a magnetic moment suggests no unpaired electron and either a d^{10} or a d^8 Pt species. The projected density of states analysis for configuration **III**, shown in Figure 9, shows fully occupied d orbitals that suggest a d^{10} species that bonds through σ_C, of CO, and a 16-electron center. This type of 16-electron center is known in organometallic chemistry,[53] and a compound of the formula, $(Cy_3P)_2Pt(CO)$, has been isolated and characterized. Pt−C and C−O bond distances for configuration **III** are 1.81 and 1.17 Å, respectively, and comparable to Pt−C and C−O distances of 1.885 and 1.131 Å reported, respectively, for $(Cy_3P)_2Pt(CO)$. Adsorption of two molecules of CO to Pt/θ-Al_2O_3 results in formation of

dx.doi.org/10.1021/ja401847c | J. Am. Chem. Soc. 2013, 135, 12634−12645

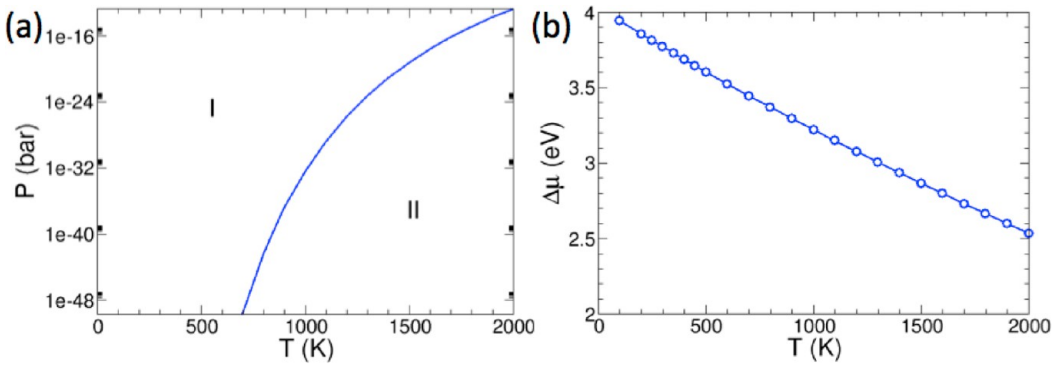

Figure 8. (a) Using a first-principles thermodynamics approach, the relative structural stabilities of configurations **I** and **II** (see Scheme 1) were calculated and the phase diagram as a function of oxygen pressure (P) and temperature (T) constructed. (b) Difference between the oxygen chemical potentials of configurations **I** and **II** at P = 1 bar.

Scheme 2. CO Adsorption on Pt/θ-Al_2O_3

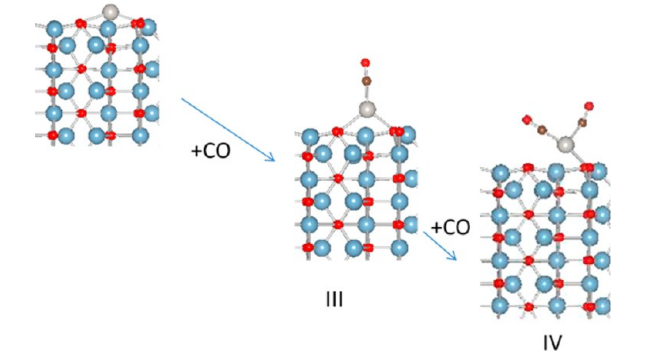

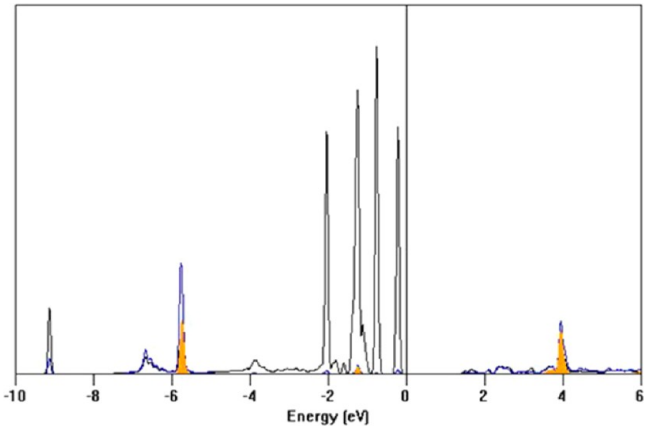

Figure 9. PDOS for Pt d orbitals (black) and carbon 2p orbitals of adsorbed CO (blue) in **III**. Filled yellow area is the contribution of p_x.

configuration **IV** with loss of one Pt to a surface oxygen bond. The two CO molecules do not bond with equal strength to platinum. Pt−C bond distances are 2.053 and 1.844 for CO cis and trans to the surface oxygen that is bonded to Pt.

There is no magnetic moment associated with **IV**, and the density of states analysis shows filled d orbitals. Thus, **IV** remains a 16-electron species where 2 electrons from the surface oxygen are replaced with 2 electrons from CO. As mentioned previously, the single supported Pt atom can be expected to be oxidized. Although DFT calculations suggest that oxygen replacement by CO is energetically feasible, our results from the all-electron DFT calculations combined with the first-principles thermodynamic approach show that once oxygen is adsorbed on Pt as in **II** it can be replaced by CO only at low oxygen pressure and very high temperatures (Figure 10).

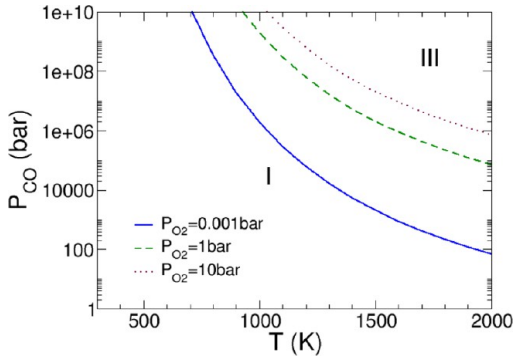

Figure 10. Phase diagram of configurations **I** and **III** (see Scheme 2) as a function of temperature (T) and CO gas pressure (P_{CO}) was obtained using the first-principles thermodynamics approach. Each line defines the phase boundary between **I** and **III**. Above the phase boundary, **III** is relatively more stable than **I** for a given oxygen pressure (P_{O2}).

This result is quite different from the conventional L−H mechanism where CO first covers Pt sites and oxygen dissociatively covers residual sites. Since CO oxidation conditions are usually at atmospheric pressure and below 225 °C (~500 K), it is unlikely that CO replaces oxygen from **I**.

In view of these results, the likely pathway for CO oxidation (Scheme 3) will involve CO adsorption on an oxidized surface resulting in intermediate **V**. Intermediate **V** in Scheme 3 is a d^{10} Pt species with filled d orbitals. The oxygen is bonded in monodentate mode, and magnetization is centered on molecular oxygen bonded to platinum. Rearrangement of **V** to a carbonate, **VI**, can occur with formation of carbon oxygen bonds between CO and the atoms of O_2. This carbonate species, **VI**, also has an analogue[54] in organometallic chemistry, $(Ph_3P)_2Pt(CO_3)$, which is a Pt(II) complex. Like $(Ph_3P)_2Pt(CO_3)$, **VI** is a 16-electron d^8 species, and density of state analysis (Figure 11) shows no electrons in Pt $5d_{xy}$ and C $2p_z$ orbitals. Loss of CO_2 from **VI** will lead to **II**, which can react with another molecule of CO to form **VII**. **VII** is a d^8 species with no magnetization associated with it, and density of states analysis shows empty $5d_{xy}$. Elimination of CO_2 from **VII** regenerates the catalyst.

dx.doi.org/10.1021/ja401847c | J. Am. Chem. Soc. 2013, 135, 12634−12645

Scheme 3. Pathway for CO Oxidation on Single Pt Atoms Supported on the (010) Surface of θ-Al_2O_3

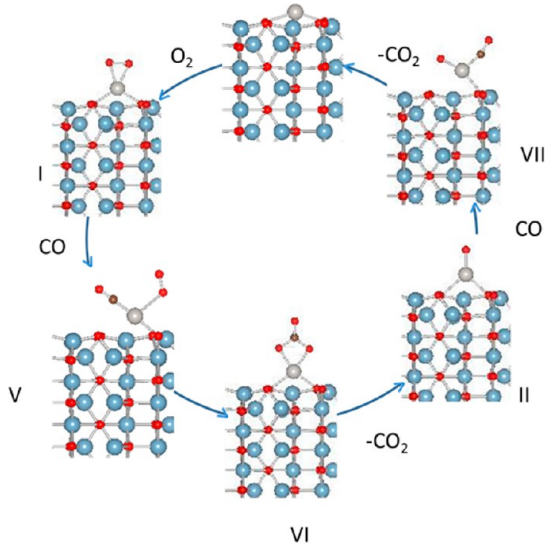

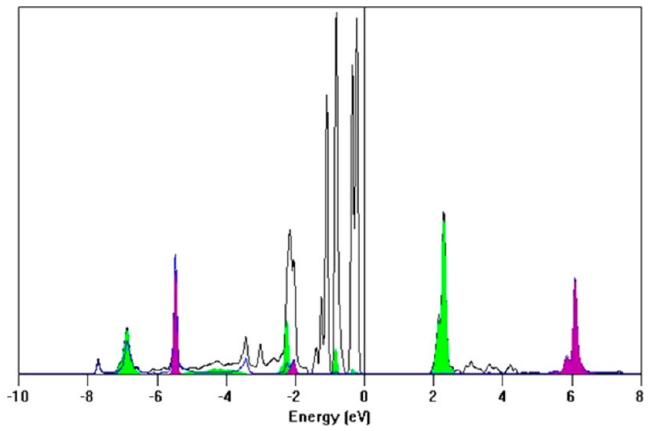

Figure 11. Density of states plots for Pt d orbitals (black) and carbon 2p orbitals of adsorbed CO (blue) in **VI**. Green and violet filled areas are for $5d_x$ and $2p_z$ contributions.

The energetics of the reactions shown in Scheme 3 can be summarized as follows

$$*Pt + O_2 \rightarrow *Pt(O_2)\,(\mathbf{I}) \quad -1.8736\text{eV}$$

$$*Pt(O_2)\,(\mathbf{I}) - O \rightarrow *Pt(O)\,(\mathbf{II}) \quad 5.6875\text{eV}$$

$$*Pt(O_2)\,(\mathbf{I}) + CO \rightarrow *Pt(O_2)(CO)\,(\mathbf{V}) \quad -1.9798\text{eV}$$

$$*Pt(O_2)(CO)\,(\mathbf{V}) \rightarrow *Pt(CO_3)\,(\mathbf{VI}) \quad -2.6396\text{eV}$$

$$*Pt(CO_3)\,(\mathbf{VI}) - CO_2 \rightarrow *Pt(O)\,(\mathbf{II}) \quad 2.2204\text{eV}$$

$$*Pt(O)\,(\mathbf{II}) + CO \rightarrow *Pt(O)(CO)\,(\mathbf{VII}) \quad -1.8102\text{eV}$$

$$*Pt(O)(CO)\,(\mathbf{VII}) - CO_2 \rightarrow *Pt \quad -1.4884\text{eV}$$

The asterisk (*) in the equations represents the support, and calculations are based on the total energies presented in Table 1. All of the reactions are energetically favorable except loss of CO_2 from **VI** which is an endothermic step. This mechanism seems to show that the surface will become covered with carbonate, unless T is high enough to dissociate it. DRIFTS experiments, described in the next section, indeed show the presence of CO_3 species. Loss of CO_2 has been previously proposed for CO oxidation on Pt nanoclusters also from an O—O—C═O species bonded to Pt nanocluster.[12] However, O—O—C═O is bonded to more than one Pt atom via O and C, which would be a less favorable configuration than **VI**. Our efforts to optimize a structure with O—O—C═O bonded to single Pt atoms were unsuccessful; the structure optimized to **V**.

Thus, the proposed mechanism shows a pathway that allows for a single supported Pt atom to be catalytically active by a modified L–H mechanism without involving the inert substrate. Considering that the supported single Pt atom is isoelectronic with organometallic species, $(Ph_3P)_2Pt$, and $(Ph_3P)_2Pt(O_2)$ and $(Ph_3P)_2Pt(CO_3)$ (analogues of proposed intermediates **I** and **VI**) have been isolated and characterized, the proposed pathway for supported single Pt atoms is quite likely.

3.4. CO Adsorption Studies. In order to obtain insights into CO oxidation pathways and obtain experimental evidence for the proposed mechanism, we carried out diffuse reflectance infrared spectroscopic (DRIFTS) studies of CO adsorption (Figure 12, left) on 0.18% and 1.0% Pt/θ-Al_2O_3.

CO adsorption on 0.18% Pt/θ-Al_2O_3 results in a broad peak in the 2300–1800 cm^{-1} range, at room temperature, with at least two identifiable peaks centered at ~2050 and ~2110 cm^{-1}. The calculated vibrational spectrum of CO adsorbed on a single supported Pt atom (**III**) is also shown in Figure 12 (right). Considering that the room-temperature spectrum of 0.18% Pt/

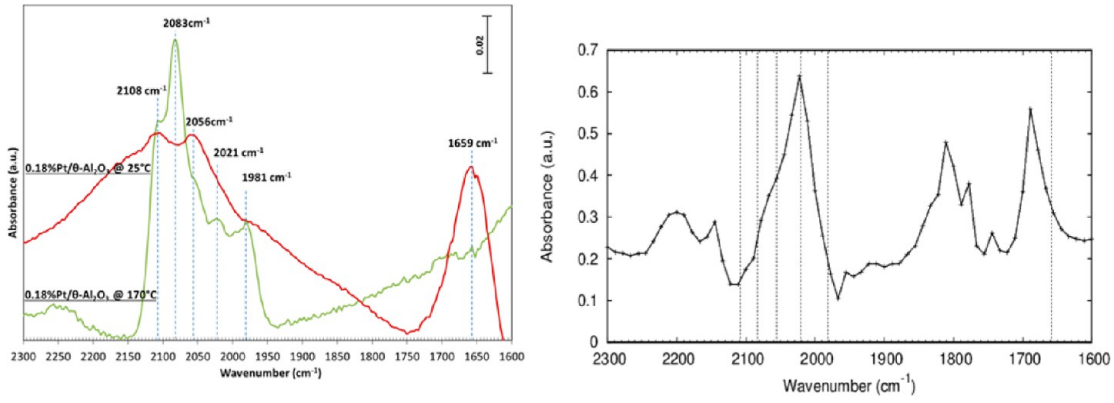

Figure 12. DRIFTS spectra of CO adsorption on 0.18% Pt/θ-Al_2O_3 at 25 and 170 °C (left), and calculated vibrational spectrum of **III**. Vertical lines correspond to the vertical lines in the observed spectrum shown on the left.

dx.doi.org/10.1021/ja401847c | J. Am. Chem. Soc. 2013, 135, 12634–12645

θ-Al_2O_3 after exposure to CO is a broad peak, we refrain from comparison of observed and calculated spectrum. As discussed in previous sections, 0.18% Pt/θ-Al_2O_3 is an oxidized species, and it is likely that its vibrational spectrum is dominated by Pt−O bonds and/or intermediates of type **V**. Increasing the temperature to 170 °C resolves the broad structure, and five peaks centered at 2108, 2083, 2056, 2021, and 1981 cm^{-1} are observed. At this temperature, CO bonds with Pt to form intermediates that contain both Pt−O and Pt−CO bonds or reacts with oxygen by releasing CO_2, thereby creating locations for Pt−CO bonds. The lack of absorption at ∼1850 cm^{-1} suggests a lack of bridging CO, which is not surprising for single Pt atoms. It should be pointed out that lack of absorption at ∼1850 cm^{-1} has also been noted previously due to low concentrations of bridging CO.[55−63] Previous assignments in the literature for supported Pt particles suggest that the 2108 cm^{-1} absorption is due to CO on Pt(II) oxide and the absorption at 2083 cm^{-1} is due to partially oxidized platinum.[55−63] Since there are no studies on IR absorption of supported single atoms on an alumina substrate, we also assign these two absorptions to Pt atoms at various stages of oxidation. The 2080 cm^{-1} absorption has previously been reported for Pt/FeO_x.[11] The features at ∼2021 and 1981 cm^{-1} have been previously reported for highly dispersed platinum supported on alumina and assigned to CO adsorbed on the metal cluster interacting with Lewis-type alumina centers.[63] In analogy with this assignment, we can assign these features to the interaction of the oxygen atom of CO adsorbed on the Pt single atoms on alumina substrate. The calculated vibrational spectrum (Figure 12, right) of CO adsorption on single supported Pt atom shows Pt−CO absorption at 2040 cm^{-1} with a shoulder at 2080 cm^{-1}. It is likely that some of the oxygen from Pt reacts with CO, forms CO_3, and is eliminated as CO_2. Under the reaction conditions, the clean Pt surface can then bond with CO. In comparison with the calculated Pt−CO frequency, we assign the peak at 2058 cm^{-1} to Pt−CO vibrations.

In comparison, the CO adsorption on 1.0% Pt/θ-Al_2O_3 at room temperature is well resolved (Figure 13) with the strongest peak at 2065 cm^{-1} and shoulders at 2118, 2104, 2083, and 1981 cm^{-1}. Since 1.0% Pt/θ-Al_2O_3 contains single atoms and 10−20 atom rafts, we expect DRIFTS to reflect absorptions from both types of platinum.

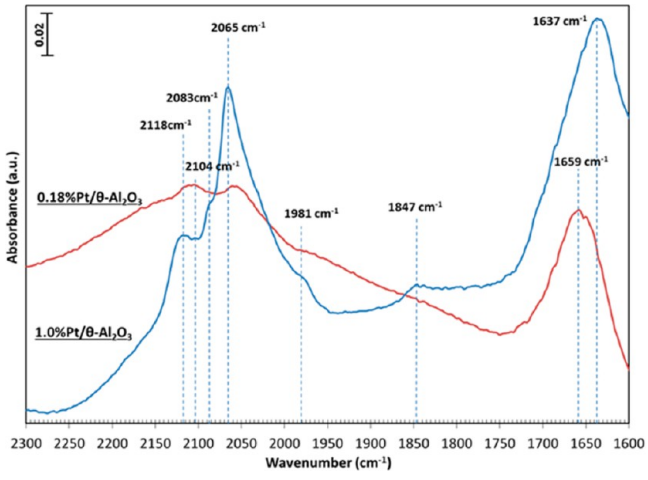

Figure 13. DRIFTS spectra of CO adsorption on 0.18% Pt/θ-Al_2O_3 and 1.0% Pt/θ-Al_2O_3 at 25 °C.

As for 1.0% Pt/θ-Al_2O_3, the 2104 and 2083 cm^{-1} absorptions can be assigned to terminal CO bonded to partially oxidized platinum while the one at 1981 cm^{-1} can be assigned to CO adsorbed on the Pt interacting with Lewis-type alumina centers.[55−63] The 2118 and 2065 cm^{-1} peaks are assigned to CO adsorbed on oxidized Pt of rafts based on literature assignments.[55−63] There is also a peak at 1847 cm^{-1} that can be assigned to bridging CO.[63] Therefore, the IR features from CO adsorbed on 1.0% Pt/θ-Al_2O_3 can be assigned as follows: absorptions at 2104, 2083, and 1981 cm^{-1} are due to the ones originating from Pt single atoms, while those at 2118, 2065, and 1847 cm^{-1} are from Pt rafts.

The proposed mechanism, described in the previous section, suggests that Pt single atoms will be covered by CO_3 unless the temperature is raised to facilitate CO_2 elimination. DRIFTS spectra of 0.18% Pt/θ-Al_2O_3 and 1.0% Pt/θ-Al_2O_3 do provide evidence for formation of a carbonate intermediate at room temperature, which supports the proposed mechanism. For 0.18% Pt/θ-Al_2O_3, after the sample has been heated at 150 °C under a flow of hydrogen and cooled to room temperature, DRIFTS shows no peaks in the carbonate region. After exposure to a flow of CO at room temperature and flushing gas-phase CO with He, a band at 1659 cm^{-1} is observed which can be assigned to bidentate CO_3 in comparison with the CO_3 band at 1672 cm^{-1} for $(Ph_3P)_2PtCO_3$.[64,65]

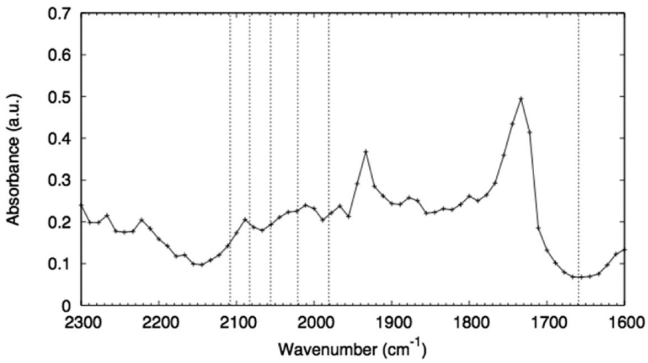

Figure 14. Calculated vibrational spectrum of VI.

The calculated vibrational spectra for **VI** shows an absorption at ∼1730 cm^{-1} which is at 71 cm^{-1} higher than the experimentally observed CO_3 vibration for 0.18% Pt/θ-Al_2O_3. Previous reports on calculated CO_3 absorption on the Pt(111) surface employing cluster models also show a deviation of 49 cm^{-1} and is considered remarkably close to the observed ones.[66] CO_3 absorption for 1.0% Pt/θ-Al_2O_3 is slightly shifted to lower wavenumbers and observed at 1637 cm^{-1}. The CO_3 band does not appear in 0.18% Pt/θ-Al_2O_3 or 1.0% Pt/θ-Al_2O_3 samples at 170 °C after exposure to flowing CO, which has been flushed with flowing helium, suggesting that CO_3 decomposes at 170 °C. We did not determine the lowest temperature at which CO_3 starts to decompose. Thus, the results of the DRIFTS study suggest that single supported atoms adsorb CO at high temperatures (CO oxidation temperature) in a linear mode and provide evidence for formation of CO_3 at room temperature, which supports the proposed mechanism.

dx.doi.org/10.1021/ja401847c | J. Am. Chem. Soc. 2013, 135, 12634−12645

4. CONCLUSIONS

We have shown that catalytically active supported single Pt atoms can be synthesized by simple solution methods on inert supports. STEM, IR, and EXAFS data show the samples to be primarily supported single Pt atoms. Previous theoretical studies had shown that such supported Pt atoms are isoelectronic with organometallic species $(Ph_3P)_2Pt$ and can be catalytically active. We find that supported Pt single atoms are indeed catalytically active as seen by facile CO oxidation. Since the broadly accepted L−H mechanism cannot operate on supported single Pt atoms, we propose a variation of the L−H mechanism to explain CO oxidation on single supported atoms on an inactive support. Two of the proposed intermediates, **I** and **VI**, in the modified L−H mechanism have well-characterized analogues in organometallic chemistry. Diffuse reflectance infrared spectroscopy shows CO absorption bands which are generally observed for CO absorption on Pt at various stages of oxidation and provide evidence for formation of CO_3 at room temperature, which supports the proposed mechanism.

■ ASSOCIATED CONTENT

Supporting Information

TOF measurements and related references, EXAFS of 0.12% Pt/θ-Al_2O_3, additional TEM data of samples, and a figure of the unit cell of *Pt(O_2). This material is available free of charge via the Internet at http://pubs.acs.org.

■ AUTHOR INFORMATION

Corresponding Author

E-mail: narulack@ornl.gov.

Notes

The authors declare no competing financial interest.

■ ACKNOWLEDGMENTS

This research was sponsored by the U.S. Department of Energy, Assistant Secretary for Energy Efficiency and Renewable Energy, Office of Vehicle Technologies, as part of the Propulsion Materials Program (C.K.N., M.M.D., M.Y., L.F.A., X.Y.) and Division of Materials Sciences and Engineering, Office of Basic Energy Sciences (G.M.S., D.R.M.), U.S. Department of Energy, under Contract DE-AC05-00OR22725 with UT-Battelle, LLC. DRIFTS and chemisorption were performed at the Center for Nanophase Materials Sciences, which is sponsored at Oak Ridge National Laboratory by the Scientific User Facilities Division, Office of Basic Energy Sciences, U.S. Department of Energy (Z.W.). EXAFS experiments were conducted at the National Synchrotron Light Source, Brookhaven National Laboratory, supported by the U.S. Department of Energy, Office of Science, Office of Basic Energy Sciences, under Contract No. DE-AC02-98CH10886 with additional support through the Synchrotron Catalysis Consortium under grant DE-FG02-05ER15688. We thank Dr. V. Schwartz for assistance with chemisorption measurements.

■ REFERENCES

(1) Heck, R. M.; Farrauto, R. J.; Gulati, S. T. *Catalytic Air Pollution Control*; Van Nostrand Reinhold: New York, 2009.
(2) Langmuir, I. *Trans. Faraday Soc.* **1921**, *17*, 621.
(3) Alavi, A.; Hu, P.; Deutsch, T.; Silvestrelli, P. L.; Hutter, J. *Phys. Rev. Lett.* **1998**, *80*, 3650.
(4) Eichler, A.; Hafner, J. *Phys. Rev. B* **1999**, *59*, 5960.
(5) Sadeghi, P.; Dunphy, K.; Punckt, C.; Rotermund, H. H. *J. Phys. Chem. C.* **2012**, *116*, 4686.
(6) Haruta, M. *Catal. Today* **1997**, *36*, 153.
(7) Abbet, S.; Heiz, U.; Hakkinen, H.; Landman, U. *Phys. Rev. Lett.* **2001**, *26*, 5950.
(8) Chen, M.; Goodman, D. W. *Science* **2004**, *306*, 252.
(9) Herzing, A. A.; Kiely, C. J.; Kiely, C. J.; Carley, A. F.; Landon, P.; Hutchings, G. J. *Science* **2008**, *321*, 1331.
(10) Turner, M. *Nature* **2008**, *454*, 981.
(11) Qiao, B.; Wang, A.; Yang, X.; Allard, L. F.; Jiang, Z.; Cui, Y.; Liu, J.; Li, J.; Zhang, T. *Nat. Chem.* **2011**, *3*, 634.
(12) Allian, A. D.; Takanabe, K.; Fujdala, K. L.; Hao, X.; Truex, T. J.; Cai, J.; Buda, C.; Neurock, M.; Iglesia, E. *J. Am. Chem. Soc.* **2011**, *133*, 4498.
(13) Uzun, A.; Ortalan, V.; Browning, N. D.; Gates, B. C. *J. Catal.* **2010**, *269*, 318.
(14) Uzun, A.; Ortalan, V.; Hao, Y.; Browning, N. D.; Gates, B. C. *ACS Nano* **2009**, *3*, 3691.
(15) Yang, X.-F.; Wang, A.; Qiao, B.; Li, J.; Liu, J.; Zhang, T. *Acc. Chem. Res.* **2013**, DOI: 10.1021/ar300361m.
(16) Yudanov, I.; Pacchioni, G.; Neyman, K.; Rosch, N. *J. Phys. Chem. B* **1997**, *101*, 2786.
(17) Heck, R. F. *Acc. Chem. Res.* **1979**, *12*, 246.
(18) Narula, C. K.; Mak, K. T.; Heck, R. F. *J. Org. Chem.* **1983**, *48*, 792.
(19) Abbet, S.; Sanchez, A.; Heiz, U.; Schneider, W.-D.; Ferrari, A. M.; Pacchioni, G.; Roesch, N. *J. Am. Chem. Soc.* **2000**, *122*, 3453.
(20) Kyriakou, G.; Boucher, M. W.; Jewell, A. D.; Lewis, E. A.; Lawron, T. J.; Baber, A. E.; Tierney, H. L.; Flytzani-Stephanopoulos, M.; Sykes, E. C. *Science* **2012**, *335*, 1209.
(21) Kwak, J. H.; Hu, J.; Mei, D.; Yi, C.-W.; Kim, D.; Peden, C. H.; Allard, L. F.; Szanyi, J. *Science* **2009**, *325*, 1670.
(22) Yates, J. T.; Worley, S. D.; Duncan, T. M.; Vaughan, R. W. *J. Chem. Phys.* **1979**, *70*, 1225.
(23) Narula, C. K.; Stocks, G. M. *J. Phys. Chem. C* **2012**, *116*, 5628.
(24) Chukhadzhyan, G. A.; Abramyan, Zh. I.; Evorkyan, G. A. *Zh. Obsh. Khim.* **1973**, *43*, 2012.
(25) Urata, H.; Tsukui, T.; Suzuki, H.; Morooka, Y.; Ikawa, T. *Chem. Lett.* **1984**, 191.
(26) Kumar, A.; Lichtenhan, J. D.; Critchlow, S. C.; Eichinger, B. E.; Borden, W. T. *J. Am. Chem. Soc.* **1990**, *112*, 5633.
(27) Narula, C. K.; Watkins, W. L. H.; Shelef, M. U.S. Patent no. 5,210,062, 1993.
(28) Leenars, A. F.; Keizer, K.; Burggraaf, A. *J. Mater. Sci.* **1984**, *19*, 1077.
(29) Nashner, M. S.; Frenkel, A. I.; Adler, D. L.; Shapley, J. R.; Nuzzo, R. G. *J. Am. Chem. Soc.* **1997**, *119*, 7760.
(30) Ravel, B.; Newville, M. *J. Synchrotron Radiat.* **2005**, *12*, 537.
(31) Wu, Z. L.; Zhou, S. H.; Zhu, H. G.; Dai, S.; Overbury, S.H. J. *Phys. Chem. C* **2009**, *113*, 3726.
(32) Kresse, G.; Hafner, J. *Phys. Rev. B* **1993**, *47*, 558.
(33) Kresse, G.; Hafner, J. *Phys. Rev. B* **1993**, *48*, 13115.
(34) Kresse, G.; Hafner, J. *Phys. Rev. B* **1994**, *49*, 14251.
(35) Perdew, J. P.; Chevary, J. A.; Vosko, S. H.; Jackson, K. A.; Pederson, M. R.; Singh, D. J. *Phys. Rev. B* **1992**, *46*, 6671.
(36) Perdew, J. P.; Chevary, J. A.; Vosko, S. H.; Jackson, K. A.; Pederson, M. R.; Singh, D. J. *Phys. Rev. B* **1993**, *48*, 4978.
(37) Bloch, P. E. *Phys. Rev. B* **1994**, *50*, 17953.
(38) Kresse, G.; Joubert, D. *Phys. Rev. B* **1999**, *59*, 1758.
(39) Blum, V.; Gehrke, R.; Hanke, F.; Havu, P.; Havu, V.; Ren, X.; Reuter, K.; Scheffler, M. *Comput. Phys. Commun.* **2009**, *180*, 2175.
(40) Perdew, J. P.; Burke, K.; Ernzerhof, M. *Phys. Rev. Lett.* **1996**, *77*, 3865. Perdew, J. P.; Burke, K.; Ernzerhof, M. *Phys. Rev. Lett.* **1997**, *78*, 1396.
(41) Yoon, M.; Weitering, H.; Zhang, Z. Y. *Phys. Rev. B* **2011**, *83*, 045413.
(42) Sinfelt, J. H.; Meitzner, G. D. *Acc. Chem. Res.* **1993**, *26*, 1.
(43) Asakura, K.; Chun, W.-J.; Shirai, M.; Tomishige, K.; Iwasawa, Y. *J. Phys. Chem B* **1997**, *101*, 5549.

(44) Panchenko, A.; Koper, M. T. M.; Shubina, T. E.; Mitchell, S. J.; Roduner, E. *J. Electrochem. Soc.* **2004**, *151*, A2016.
(45) Anderson, A. B.; ALbu, T. V. *J. Electrochem. Soc.* **2000**, *147*, 4229.
(46) Jacob, T.; Muller, R. P.; Goddard, W. A., III *J. Phys. Chem. B* **2003**, *107*, 9465.
(47) Eichler, A.; Hafner, J. *Phys. Rev. Lett.* **1997**, *79*, 4481.
(48) Luntz, A. C.; Grimblot, J.; Fowler, D. E. *Phys. Rev. B* **1989**, *39*, 12903.
(49) Xiao, L.; Schneider, W. F. *Chem. Phys. Lett.* **2010**, *484*, 231.
(50) Cheng, P.-T.; Cook, C. D.; Nyburg, S. C.; Wan, K. Y. *Can. J. Chem.* **1971**, *49*, 3772.
(51) Sakaki, S.; Hori, K.; Ohyohi, A. *Inorg. Chem.* **1978**, *17*, 3183.
(52) Xu, Y.; Shelton, W. A.; Schneider, W. F. *J. Phys. Chem. B* **2006**, *110*, 16591.
(53) Bertsch, S.; Braunschweig, H.; Forster, M.; Gruss, K.; Radacki, K. *Inorg. Chem.* **2011**, *50*, 1816.
(54) Gregg, M. R.; Powell, J.; Sawyer, J. F. *Acta Crystallogr.* **1988**, *C44*, 43.
(55) Von Oertzen, A.; Rotermund, H. H.; Nettesheim, S. *Surf. Sci.* **1994**, *311*, 322.
(56) Spiel, C.; Vogel, D.; Suchorski, Y.; Drachsel, W.; Schoegl, R.; Rupprechter, G. *Catal. Lett.* **2011**, *141*, 625.
(57) Gritsch, T.; Coulman, D.; Behm, R. J.; Ertl, G. *Phys. Rev. Lett.* **1989**, *63*, 1086.
(58) Primet, M.; Basset, J. M.; Mathieu, M. V.; Prette, M. *J. Catal.* **1973**, *29*, 213.
(59) Sheppard, N.; Nguyen, T. T. *Adv. Infrared Raman Spectrosc.* **1978**, *5*, 67.
(60) Haaland, D. M.; Williams, F. L. *J. Catal.* **1982**, *76*, 450.
(61) Primet, M. *J. Catal.* **1984**, *88*, 273.
(62) Andersson, J. A.; Rochester, C. H. *J. Chem. Soc., Faraday Trans.* **1991**, *87*, 1479.
(63) Menorval, L.-C.; Chaqroune, A.; Coq, B.; Figueras, F. *J. Chem. Soc., Faraday Trans.* **1997**, *93*, 3715.
(64) Hayward, P. J.; Blake, D. M.; Wilkinson, G.; Nyman, C. J. *J. Am. Chem. Soc.* **1970**, *92*, 5873.
(65) Balema, V. P.; Wiench, J. W.; Pruski, M.; Pecharsky, V. K. *Chem. Commun.* **2002**, 1606.
(66) Markovits, A.; Garcia-Hernandez, M.; Ricart, J. M.; Illas, F. *J. Phys. Chem. B* **1999**, *103*, 509.